Missing Fe: hydrogenated iron nanoparticles

G. Bilalbegović[1], A. Maksimović[2], V. Mohaček-Grošev[2]
[1]*Department of Physics, Faculty of Science, University of Zagreb, Bijenička 32, 10000 Zagreb, Croatia*
[2]*Center of Excellence for Advanced Materials and Sensing Devices, Rudjer Bošković Institute, Bijenička 54, 10000 Zagreb, Croatia*

2 November 2016

ABSTRACT
Although it was found that the FeH lines exist in the spectra of some stars, none of the spectral features in the ISM have been assigned to this molecule. We suggest that iron atoms interact with hydrogen and produce Fe-H nanoparticles which sometimes contain many H atoms. We calculate infrared spectra of hydrogenated iron nanoparticles using density functional theory methods and find broad, overlapping bands. Desorption of H_2 could induce spinning of these small Fe-H dust grains. Some of hydrogenated iron nanoparticles posses magnetic and electric moments and should interact with electromagnetic fields in the ISM. Fe_nH_m nanoparticles could contribute to the polarization of the ISM and the anomalous microwave emission. We discuss the conditions required to form FeH and Fe_nH_m in the ISM.

Key words: ISM: molecules – ISM: lines and bands – astrochemistry – methods: numerical – ISM: magnetic fields – stars: individual: IRC+10216

1 INTRODUCTION

Iron is one of the most abundant chemical elements on Earth and in the Galaxy. It is proposed that more than 65% of Fe is injected as gas into the ISM (Dwek 2016). However, it is known that iron is strongly depleted (Savage & Bohlin 1979; Jensen & Snow 2007; Delgado Inglada et al. 2009; Jenkins 2009; Jones 2014; Dwek 2016). Therefore, it was suggested that Fe atoms hide in dust grains. Although the number of known molecules in the ISM approaches two hundreds (Tielens 2013), only two chemical species containing iron have been detected: FeO and FeCN (Endres et al. 2016; Walmsley et al. 2002; Furuya et al. 2003; Zack, Halfen & Ziurys 2011). Therefore, the search for additional iron species in the ISM and cosmic dust is necessary.

The most abundant element in the universe is hydrogen. It is important to consider chemical compounds consisting of iron and hydrogen. The FeH molecule has been discussed in the astrophysical literature. It was proposed that FeH forms in the Sun and some other stars (Carroll, McCormack & O'Connor 1976). The spectrum of several stars in the ultraviolet, visible, and near-infrared region was compared with laboratory measurements of FeH and good agreement for some lines was obtained. The near-infrared Wing-Ford band at 0.99 μm was connected with the FeH spectral features in S stars, M-type giants, M and L dwarfs (Nordh, Lindgren & Wing 1977; Wing, Cohen & Brault 1977; Clegg & Lambert 1978; Jones et al. 1996; Kirkpatrick et al. 1999; McLean et al. 2000; Buenzli et al. 2015). The extensive literature about FeH is available on the ExoMol web page: http://www.exomol.com/bibliography/FeH (Tennyson & Yurchenko 2012).

Studies in materials science have shown that the Fe atom and small iron clusters could bind many hydrogen atoms (Whetten et al. 1985; Richtsmeier et al. 1985; Parks et al. 1985; Knickelbein et al.

1998; Wang & Andrews 2009; Takahashi, Isobe & Ohnuki 2013). It was suggested that hydrogen atoms chemisorb on Fe_n in the first step. Additional hydrogen atoms are attached by physisorption in the second step. Therefore, complexes and supercomplexes containing one, or a few, Fe atoms and many H atoms are formed. We study hydrogenated iron nanoparticles to shed light on the missing cosmic iron problem.

2 COMPUTATIONAL METHODS

We use density functional theory (DFT) methods (Becke 2014; Jones 2015). In DFT the total energy of a quantum system is determined by the electron density $n(\vec{r}) = \Sigma|\psi(\vec{r})|^2$ of the ground state. By using various physical and computational algorithms DFT gives a realistic description of many physical and chemical properties of nuclei, atoms, molecules, nanoparticles, and solids.

Results are obtained by the GPAW code (Enkovaara et al. 2010) and its ASE user interface (Bahn & Jacobsen 2002). The generalized Gradient Approximation (GGA) (Perdew, Burke & Ernzerhof 1997) in its spin-polarized form is chosen, as well as the PAW pseudopotentials (Mortensen, Hansen & Jacobsen 2005). We start from Fe-H nanoparticles first optimized globally, and then using GPAW DFT methods, by Takahashi and coworkers (Takahashi, Isobe & Ohnuki 2013; Takahashi 2014). However, we use the newest version of the GPAW package and reoptimize structures for the grid spacing of 0.14 Å. Takahashi and coworkers investigated structural properties and bonding of Fe-H nanoparticles. They also reported magnetic moments for a few of Fe-H clusters. We are interested in astrophysical applications. In this work we calculate infrared (IR) spectra, electric and magnetic moments of hydrogenated iron nanoparticles. IR spectra are obtained using the

finite-difference approximation for a dynamical matrix and the gradient of the dipole momentum (Porezag & Pederson 1996; Frederiksen et al. 2007). The IR intensity I_i of the mode i is obtained using

$$I_i = \frac{N\pi}{3c}\left|\frac{d\vec{\mu}}{dQ_i}\right|^2,$$

where N is the particle density, c is the velocity of light, μ is the electric dipole momentum, and Q_i is the coordinate of the normal mode. The same DFT code and similar computational methods in calculations of IR spectra of cement (Ca-Si-O-H) nanoparticles with astrophysical applications(Bilalbegović, Maksimović & Mohaček-Grošev 2014) produced good agreement with measured IR spectra of the cement paste (Garbev et al. 2007). The IR frequencies we calculate correspond to stretching and bending modes in nanoparticles. Calculated data are absorption spectra and they are convolved with the Lorentzian band profiles to adjust them to astronomical emission spectra (Bauschlicher et al. 2010). These vibrational modes are excited when nanoparticles are heated by starlight and their main excitation mechanism is the absorption of a UV photon. Excited nanoparticles relax by IR emission. However, hydrogenated iron nanoparticles could also form or adsorb onto dust grains where they could be seen in absorption.

Figure 1. The optimized structures of: (a) FeH_{10}, (b) Fe_9H_{56}. Fe and H atoms are represented by the red and blue circles, respectively.

Figure 2. The optimized structures of: (a) Fe_3H_{25}, (b) Fe_4H_{25}. Fe and H atoms are represented by the red and blue circles, respectively.

3   RESULTS AND DISCUSSION

3.1   IR spectra of hydrogenated iron nanoparticles

We present here IR spectra for four typical examples of hydrogenated iron nanoparticles shown in Figs. 1 and 2. FeH_{10} (Fig. 1 (a)) is the structure with the largest number of hydrogen atoms connected to the single Fe atom we investigated. Fe_9H_{56} (Fig. 1 (b)) is the hydrogenated iron nanoparticle with the largest number of atoms we studied. Much larger Fe_nH_m nanoparticles, with n up to 130, were investigated in experiments (Parks et al. 1985). In the Supporting Information we also show IR spectra for Fe_3H_{25} (Fig. 2 (a)) and Fe_4H_{25} (Fig. 2 (b)) to compare two structures with the same number of hydrogen atoms bonded to Fe_n and Fe_{n+1}. The Lorentzian profiles with a full width at half-maximum of 20 cm^{-1} are used for IR bands presented in Figs. 3 and Fig. S1 in the Supporting Information. Tables of bands and their intensities for these structures are available in the Supporting Information. For some Fe-H nanoparticles the spectrum extends to the far IR. For example, bands of Fe_4H_{25} draw out above 100 μm (see Fig. S1 (d) in the Supporting Information).

Knickelbein et al. (1998) carried out an experimental study of multiply hydrogenated iron nanoparticles, F_nH_m, $n = 9 - 20$. IR spectra were recorded in the (9.2-11.3) μm region. They found that bands overlap and that each band is about 20 cm^{-1} in width. They also carried DFT calculations using the local spin density approximation for only one cluster: $Fe_{13}H_{14}$. This structure was constructed to have Th symmetry of the iron core. Its theoretical IR spectrum was much simpler than measured spectra showing that real hydrogenated iron nanoparticles have low symmetry. In agreement with experimental results of Knickelbein et al. (1998), we optimize structures with low symmetry and find that their IR bands often overlap. It could be difficult to disentangle some of these IR features from those of other species in the space.
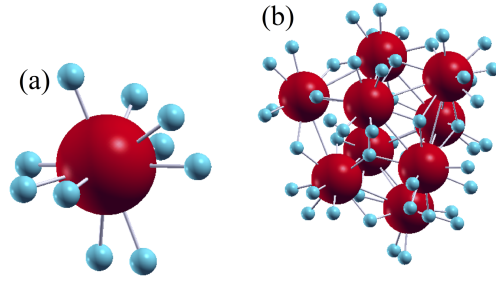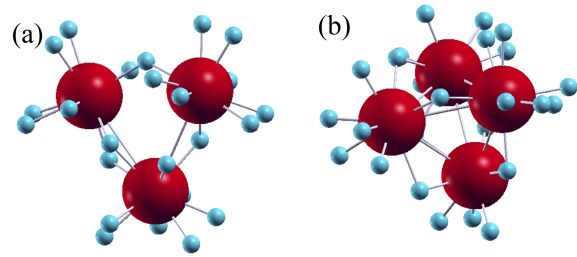
3.2   Hydrogenated iron nanoparticles and the interstellar electromagnetic fields

Some of Fe-H nanoparticles have electric and magnetic moments. For example, we calculate magnetic moments of: $4\mu_B$ (FeH_2), 0 μ_B (FeH_{10}), 0 μ_B (Fe_9H_{56}). Starting from FeH_2, magnetic moments for FeH_m decrease with m in the oscillatory way. For Fe_8H_{51} we calculate 1 μ_B. For Fe_3H_{25} and Fe_4H_{25} (shown in Fig. 2) we find magnetic moments of -1 μ_B and +1 μ_B, respectively. All magnetic and electric dipole moments we calculate are shown in Table 1. The values of electric moments fluctuate between zero and 2.6 D. The values of all magnetic moments in Table 1 are rather low. However, Knickelbein (2002) carried out magnetic measurements
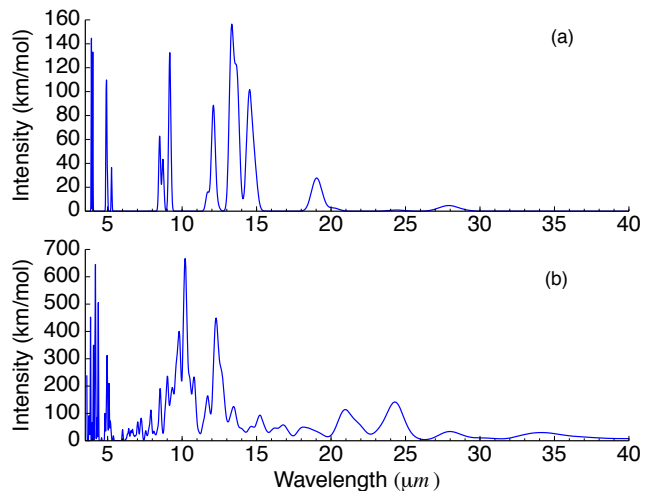
Figure 3. IR spectra of: (a) FeH_{10}, (b) Fe_9H_{56}.

Table 1. Calculated magnetic (M) and electric dipole (μ) moments for Fe-H species.

System	M (μ_B)	μ (D)
FeH_2	4	0
FeH_3	3	2.361
FeH_4	2	2.553
FeH_5	1	1.339
FeH_6	2	0.125
FeH_7	1	0.779
FeH_8	2	0.025
FeH_9	1	1.040
FeH_{10}	0	1.232
Fe_2H_{18}	0	1.510
Fe_3H_{25}	1	0.675
Fe_4H_{25}	1	1.012
Fe_5H_{28}	0	1.218
Fe_6H_{32}	0	0.611
Fe_7H_{39}	1	1.429
Fe_8H_{51}	1	2.324
Fe_9H_{56}	0	0.454

on Fe_n and Fe_nH_m, $n = 10 - 25$, nanoparticles and found that hydrogenation substantially increases magnetic moments of iron clusters for $n \geqslant 13$. The largest enhancement was measured for $n = 13$. All n values between 13 and 18 also show big enhancements. Magnetic moments of F_nH_m, $n = 13 - 18$, were (4-5) μ_B, whereas the corresponding values for Fe_n were (2-3) μ_B (Knickelbein 2002). It is possible to expect that the most pronounced interaction with the magnetic field occurs for hydrogenated iron dust grains of this size. Other intervals of enhancements for magnetic moments of F_nH_m (for $n > 25$) are also possible.

Therefore, some of Fe_nH_m nanoparticles interact with the cosmic electromagnetic field. The alignment of interstellar grains is well known problem (Andersson, Lazarian & Vaillancourt 2015). Various mechanisms of this alignment have been discussed for some time. Present understanding is that larger dust grains are aligned because of radiative processes, whereas alignment by a paramagnetic relaxation is feasible for small grains. The 2175 Å extinction bump was attributed to PAH (Polycyclic Aromatic Hydrocarbon) molecules (Steglich et al. 2011). It was found that this 2175 Å feature shows polarization (Martin, Clayton & Wolff 1999). Therefore, it is important to study magnetic properties and polarization of the smallest dust grains, such as PAHs and Fe-H nanoparticles. The alignment of silicate grains with inclusions in the form of iron nanoparticles was recently investigated (Hoang & Lazarian 2016). Most of previous studies on alignment of silicate grains with Fe were based on the model where iron atoms are distributed diffusively. It was found that iron nanoparticles inclusions in grains can enhance their alignment. The core of iron atoms is also present in the Fe_nH_m nanoparticles.

It is important to consider a possible photodestruction of Fe_nH_m. Similar problems, i.e., loss of aromatic H and side-groups, have been studied for PAHs (Tielens 2005). Reaction rates for these processes have been evaluated within several models (RRK, RRKM, RKM, QRKM). Because of the exponential dependence, small errors in the energies and entropies in unimolecular reactions produce large errors in the reaction rates. Therefore, better solutions are based on experimental data (Tielens 2005). Hydrogenated iron nanoparticles are much less studied than PAHs, for which plenty of data accumulated for a long time in chemistry and physics, as well as over last thirty years in astrophysics. However,

Parks et al. (1987) found that multiphoton absorption for hydrogenated iron nanoparticles leads primarily to loss of hydrogen adsorbates because of the less energy this process takes in a comparison with breaking a metal-metal bond. One-photon fragmentation was also observed in a few cases.

Liu et al. (1985) found that the laser-induced multiphoton absorption on hydrogenated iron nanoparticles leads to desorption of a specific number of H_2 molecules. The desorption energy of 1.3 eV was estimated, but it was also found that this value slightly depends on the coverage. They also analyzed their experimental results within the RRKM model (Liu et al. 1985). In experiments on hydrogen-saturated iron nanoparticles Knickelbein et al. (1998) observed that the laser-induced heating below 150K leads to a loss of some of the physisorbed H_2 molecules. UV lasers were used in experiments on photodestruction of Fe_nH_m (Parks et al. 1987; Liu et al. 1985; Knickelbein et al. 1998). The strength of the FUV interstellar field is 1.7 (Draine 1978), or 1.6 (Parravano, Hollenbach & McKee 2003), times greater than the Habing field of 1.6×10^{-3} erg $cm^{-2} s^{-1}$. Therefore, desorption, induced by radiation and heating, could occur in the ISM. It was suggested that the H_2 desorption from small dust grains could induce their spinning (Mathis 1986).

The anomalous microwave emission (AME) is the excess emission observed in the (10-60) GHz frequency range (Kogut et al. 1996; Leitch et al. 1997; Dickinson, Paladini & Verstraete 2013). Electric dipole emission from spinning small dust grains (Draine & Lazarian 1998) and magnetic dipole emission from magnetic nanoparticles (Draine & Lazarian 1999) were proposed as the source of the AME. PAHs are often studied as such very small grains. By analyzing full-sky observations in the IR and microwave region from the Planck Collaboration (Planck Collaboration et al. 2014), Hensley, Draine & Meisner (2016) found that there is no correlation between fluctuations of the AME intensity and fluctuations in the emission of PAHs. Other carriers, such as nanosilicates (Hoang, Vinh & Lan 2016), were recently proposed for a possible orgin of the AME. Fe-H nanoparticles could be also present in the ISM and their spinning, electric and magnetic emissions could be one of sources of the AME.

3.3 *Astrophysical Origin*

FeH molecules have been seen in brown dwarfs, S stars and M-type giants till now. Brown dwarfs do not have typical stellar winds and the amount of FeH molecules they could inject to the ISM is small. However, S stars and M giants do have pronounced winds (Ramstedt, Schöier & Olofsson 2009; Ferrarotti & Gail 2002; Kudritzki & Reimers 1978) and could inject FeH to the ISM. The presence of FeH in S stars and M giants is discussed in Wing (1972); Nordh, Lindgren & Wing (1977); Clegg & Lambert (1978); Lambert (1988); Hirai & Chinami (1992). Mould & Wyckoff (1978) calculated column densities of FeH for several models of stellar atmospheres for S and M stars. This calculation was updated by Lambert & Clegg (1980). The values at 3000 K are: log N = 15.3 for the M giant (C/O=0.6), log N = 15.8 for the S star (C/O=0.98), log N = 15.9 for the S star (C/O=1).

It is known that PAHs are destroyed in the ISM by shocks (Micelotta, Jones & Tielens 2010b), in a hot post-shock gas (Micelotta, Jones & Tielens 2010a), and by cosmic rays (Micelotta, Jones & Tielens 2011). The PAHs injection time to the ISM is longer than a timescale for their destruction. The same problem exists for interstellar dust grains (Jones et al. 1994). It was suggested that PAHs and grains reform in the ISM. An efficient process is condensation on already existing grains (Jones et al. 1994; Dwek

2016). Similar mechanisms play a role in the destruction and replenishment of hydrogenated iron nanoparticles.

Bar-Nun, Pasternak & Barrett (1980) suggested that FeH and FeH$_2$ may form on grain surfaces in very cold interstellar clouds. After performing and analyzing laboratory astrophysical experiments, they proposed that H atoms diffuse and react with Fe atoms adsorbed on the graphite, silicate or icy grains at low temperatures. The energy of 1.7 eV released in the chemical reaction Fe + H $\rightarrow$ FeH is absorbed by a grain. The ejection of FeH and FeH$_2$ from grains by cosmic rays and sputtering during cloud collisions was proposed. Hydrogenated iron species could be also ejected from very small grains by the energy released from chemical reactions during the bond formation (Bar-Nun, Pasternak & Barrett 1980). Recent DFT and experimental studies have shown that hydrogenation of Fe nanoparticles is preserved on a single layer graphene supported by the Cu substrate (Takahashi et al. 2014). Iron nanoparticles were deposited by vacuum deposition and hydrogenation was done with hydrogen gas under 1 atm and at the liquid nitrogen temperature. The copper substrate (on which a graphene layer is physisorbed) was chosen because of commercial applications (Takahashi et al. 2014). We expect that some other substrates, including cosmic dust grains, show similar properties, i.e. support and preserve hydrogenation of iron nanoparticles under suitable conditions. For example, Navarro-Ruiz et al. (2016) studied the formation of H$_2$ on Fe-containing olivine-based interstellar grains using DFT methods. They found that H adsorption on Fe sites is much stronger than on Mg ones. Because of the strong chemisorbed Fe-H bond, Fe-containing olivines can capture hydrogen atoms on an astronomical time scale. Using computational methods Fioroni & DeYonker (2016) studied the H$_2$ formation on siliceous surfaces grafted with Fe$^+$. It was found that Fe-H and Fe-H$_2$ formation is always thermodynamically favored. The H atom remains on the Fe-H center increasing the probability for a second atom to react. Therefore, hydrogenated iron nanoparticles could form at S stars, M giants, and on dust grains in the ISM.

IRC +10216 (CW Leo) is the nearby, asymptotic giant branch evolved carbon star known as one of the brightest mid-IR sources outside the Solar system. More than 80 molecular species, as well as many unidentified lines, have been detected in IRC +10216 (Cernicharo et al. 1996; Monnier et al. 2000; Mauron & Huggins 2010; Tenenbaum et al. 2010; Agúndez et al. 2012; Cernicharo et al. 2013; Gong et al. 2015). Gas phase iron in significant abundance was detected in the circumstellar envelope of IRC +10216 with the UVES spectrograph (Mauron & Huggins 2010). Observed column densities of refractory metals indicated that iron and other such elements are not completely removed from the gas phase by dust condensation. The FeCN molecule was detected in IRC +10216 (Zack, Halfen & Ziurys 2011), as well as several other molecules containing metals. Therefore, we suggest that IRC +10216 is one of astrophysical environments where hydrogenated iron nanoparticles may form. The upper limit of 10^{-9} (relative to H$_2$) to the FeH abundance in IRC +10216 was proposed, under the assumption that the emitting region has an average kinetic temperature of 300 K (Cernicharo et al. 2010). Ozin & McCaffrey (1984), as well as Rubinovitz & Nixon (1986), found that UV radiation promotes the formation of FeH$_2$. We expect that the formation of hydrogenated iron nanoparticles is efficient in astrophysical environments with UV radiation.

4 CONCLUSIONS

It is very important to study iron and its compounds in order to understand the properties of cosmic dust and molecules in the ISM. While pure iron, its oxides and sulfides, were discussed as components of cosmic dust grains, Fe-H nanoparticles were not studied in the astrophysical literature, to the best of our knowledge. We studied hydrogenated iron nanoparticles to point out their possible role in the balance of iron and hydrogen in the ISM. Fe atoms are sometimes surrounded with many hydrogen atoms. Therefore, it is difficult for iron atoms in the core to interact with non-hydrogen atoms. This could explain why only two molecules containing iron atoms were detected in the space till now. We use density functional theory methods and calculate IR spectra of Fe-H nanoparticles, their electric and magnetic moments. The IR spectrum of hydrogenated iron nanoparticles consists of broad, overlapping bands that could be difficult to separate from those of other species in the ISM. We propose observations in the radio, optical and UV spectral regions as additional, and perhaps better, tests for detection of hydrogenated iron nanoparticles in the ISM. Hydrogenated iron nanoparticles with electric and magnetic moments interact with cosmic electromagnetic fields. In addition, H$_2$ molecules could desorbe from highly hydrogenated nanoparticles yielding to their spinning. Therefore, hydrogenated nanoparticles are good candidates for the analysis of processes such as the alignment of interstellar grains and the anomalous microwave emission. We suggest S stars and M giants, as well as IRC +10216, as astrophysical sources where the search for hydrogenated iron nanoparticles could start. New experimental, theoretical, and observational studies are needed to reveal a role of hydrogenated iron nanoparticles in the ISM.

REFERENCES

Agúndez M., Fonfría J. P., Cernicharo J., Kahane C., Daniel F., Guélin M., 2012, AA, 543, A48

Andersson B. G., Lazarian A., Vaillancourt J. E., 2015, ARAA, 53, 501

Bahn S. R., Jacobsen K. W., 2002, Comput. Sci. Eng., 4, 56

Bar-Nun A., Pasternak M., Barrett P. H., 1980, AA, 87, 328

Bauschlicher C. W. et al., 2010, ApJS, 189, 341

Becke A. D., 2014, J. Chem. Phys., 301, 5648

Bilalbegović G., Maksimović A., Mohaček-Grošev V., 2014, MNRAS, 442, 1319

Buenzli E., Marley M. S., Apai D., Saumon D., Biller B. A., Crossfield, M. I. J., Radigan J., 2015, ApJ, 812, 163

Carroll P. K., McCormack P., O'Connor S., 1976, ApJ, 208, 903

Cernicharo J. et al., 1996, AA, 315, L201

Cernicharo J., Daniel F., Castro-Carrizo A., Agundez M., Marcelino N., Joblin C., Goicoechea J. R., Guélin M., 2013, ApJL, 778, L25

Cernicharo J. et al., 2010, AA, 518, L136

Clegg R. E. S., Lambert D. L., 1978, ApJ, 226, 931

Delgado Inglada G., Rodriguez M., Mampaso A., Viironen K., 2009, ApJ, 694, 1335

Dickinson C., Paladini R., Verstraete L., 2013, AdAst, 2013, 1

Draine B. T., 1978, ApJS, 36, 595

Draine B. T., Lazarian A., 1998, ApJ, 508, 157

Draine B. T., Lazarian A., 1999, ApJ, 512, 740

Dwek E., 2016, ApJ, 825, 136

Endres C. P., Schlemmer S., Schilke P., J. S., Müller H. S. P., 2016, J. Mol. Spectrosc., 327, 95

Enkovaara J. et al., 2010, J. Phys.: Cond. Matt., 22, 253202

Ferrarotti A. S., Gail H.-P., 2002, AA, 382, 256

Fioroni M., DeYonker N. J., 2016, Chem. Commun.

Frederiksen T., Paulsson M., Brandbyge M., Jauho A. P., 2007, Phys. Rev. B, 75, 205413

Furuya R. S., Walmsley C. M., Nakanishi K., Schilke P., Bachiller R., 2003, AA, 409, L21

Garbev K., Stemmermann P., Black L., Breen C., Yarwood J., Gasharova B., 2007, J. Am. Ceram. Soc., 90, 900

Gong Y., Henkel C., Spezzano S., Thorwirth S., Menten K. M., Wyrowski F., Mao R. Q., Klein B., 2015, AA, 574, A56

Hensley B. S., Draine B. T., Meisner A. M., 2016, ApJ, 827, 45

Hirai M., Chinami K., 1992, Proc. Jpn. Acad. Ser. B Phys. Biol. Sci., 68, 4

Hoang T., Lazarian A., 2016, arXiv:1605.02828

Hoang T., Vinh N. A., Lan N. Q., 2016, ApJ, 824, 18

Jenkins E. B., 2009, ApJ, 700, 1299

Jensen A. G., Snow T. P., 2007, ApJ, 669, 378

Jones A., 2014, in The Life Cycle of Dust in the Universe: Observations, Theory, and Laboratory Experiments, Andersen A., Baes M., Gomez H., Kemper C., Watson D., eds. No. PoS(LCDU2013)001, arXiv:1411.6666, Proceedings of Science, SISSA, Trieste

Jones A. P., Tielens A. G. G. M., Hollenbach D. J., McKee C. F., 1994, ApJ, 433, 797

Jones H. R. A., Longmore A. J., Allard F., Hauschildt P. H., 1996, MNRAS, 280, 77

Jones R. O., 2015, Rev. Mod. Phys., 87, 897

Kirkpatrick J. D., Allard F., Bida T., Zuckerman B., Becklin E. E., Chabrier G., Baraffe I., 1999, ApJ, 519, 834

Knickelbein M. B., 2002, Chem. Phys. Lett., 353, 221

Knickelbein M. B., Koretsky G. M., Jackson K. A., Pederson M. R., Hajnal Z., 1998, J. Chem. Phys., 109, 10692

Kogut A., Banday A. J., Bennett C. L., Gorski K. M., Hinshaw G., Smoot G. F., Wright E. I., 1996, ApJL, 464, L5

Kudritzki R. P., Reimers D., 1978, AA, 70, 227

Lambert D. L., 1988, PASP, 100, 1202

Lambert D. L., Clegg R. E. S., 1980, MNRAS, 191, 367

Leitch E. M., Readhead A. C. S., Pearson T. J., Myers S. T., 1997, ApJ, 486, L23

Liu K., Parks E. K., Richtsmeier S. C., Pobo L. G., Riley S. J., 1985, J. Chem. Phys., 83, 2882

Martin P. G., Clayton G. C., Wolff M. J., 1999, ApJ, 510, 905

Mathis J. S., 1986, ApJ, 308, 281

Mauron N., Huggins P. J., 2010, AA, 513, A31

McLean I. S. et al., 2000, ApJL, 533, L45

Micelotta E. R., Jones A. P., Tielens A. G. G. M., 2010a, AA, 510, A37

Micelotta E. R., Jones A. P., Tielens A. G. G. M., 2010b, AA, 510, A36

Micelotta E. R., Jones A. P., Tielens A. G. G. M., 2011, AA, 526, A52

Monnier J. D., Danchi W. C., Hale D. S., Tuthill P. G., Townes C. H., 2000, ApJ, 543, 868

Mortensen J. J., Hansen L. B., Jacobsen K. W., 2005, Phys. Rev. B, 71, 035109

Mould J. R., Wyckoff S., 1978, MNRAS, 182, 63

Navarro-Ruiz J., Ugliengo P., Sodupe M., Rimola A., 2016, Chem. Commun., 52, 6873

Nordh H. L., Lindgren B., Wing R. F., 1977, AA, 56, 1

Ozin G. A., McCaffrey J. G., 1984, J. Phys. Chem., 88, 645

Parks E. K., Liu K., Richtsmeier S. C., Pobo L. G., Riley S. J., 1985, J. Chem. Phys., 82, 5470

Parks E. K., Nieman G. C., Pobo L. G., Riley S. J., 1987, J. Phys. Chem., 91, 2671

Parravano A., Hollenbach D. J., McKee C. F., 2003, ApJ, 584, 797

Perdew J. P., Burke K., Ernzerhof M., 1997, Phys. Rev. Lett., 78, 1396

Planck Collaboration et al., 2014, AA, 565, A103

Porezag D., Pederson M. R., 1996, Phys. Rev. B, 54, 7830

Ramstedt S., Schöier F. L., Olofsson H., 2009, AA, 499, 515

Richtsmeier S. C., Parks E. K., Liu K., Pobo L. G., Riley S. J., 1985, J. Chem. Phys., 82, 3659

Rubinovitz R. L., Nixon E. R., 1986, J. Phys. Chem., 90, 1940

Savage B. D., Bohlin R. C., 1979, ApJ, 229, 136

Steglich M., Bouwman J., Huisken F., Henning T., 2011, ApJ, 742, 2

Takahashi K., 2014, PhD thesis, Hokkaido University

Takahashi K., Isobe S., Ohnuki S., 2013, Appl. Phys. Lett., 102, 113108

Takahashi K., Wang Y., Chiba S., Nakagawa Y., Isobe S., Ohnuki S., 2014, Sci. Rep., 4, 4598

Tenenbaum E. D., Dodd J. L., Milam S. N., Woolf N. J., Ziurys L. M., 2010, ApJS, 190, 348

Tennyson J., Yurchenko S. N., 2012, MNRAS, 425, 21

Tielens A. G. G. M., 2005, The Physics and Chemistry of the Interstellar Medium. Cambridge University Press

Tielens A. G. G. M., 2013, Rev. Mod. Phys., 85, 1021

Walmsley C. M., Bachiller R., Pineau des Forêts G., Schilke P., 2002, ApJ, 566, L109

Wang X., Andrews L., 2009, J. Phys. Chem. A, 113, 551

Whetten R. L., Cox D. M., Trevor D. J., Kaldor A., 1985, Phys. Rev. Lett., 54, 1494

Wing R. F., 1972, in Les Spectres des Astres dans l'Infrarouge et les Microondes, pp. 123–140

Wing R. F., Cohen J., Brault J. W., 1977, ApJ, 216, 659

Zack L. N., Halfen D. T., Ziurys L. M., 2011, ApJ, 733, L36

Supporting Information

Table S1. Infrared bands and intensities for FeH$_{10}$. Only bands with intensities above 2 km mol^{-1} are shown.

Band (μm)	Intensity (km mol^{-1})
27.907	4.740
20.185	2.570
19.197	13.425
19.064	2.969
18.885	14.827
14.855	34.916
14.508	95.236
13.684	109.959
13.317	148.760
12.376	4.460
12.097	88.331
11.709	15.564
9.172	132.600
8.713	43.290
8.493	62.783
5.290	4.042
5.263	34.319
4.994	26.525
4.975	3.186
4.936	91.542
4.896	84.764
4.004	133.180
3.922	100.403
3.902	92.107

Table S2. Infrared bands and intensities for Fe_9H_{56}. Only bands with intensities above 2 km mol^{-1} are shown.

| Band (μm)	Intensity (km mol^{-1})	Band (μm)	Intensity (km mol^{-1})	Band (μm)	Intensity (km mol^{-1})	Band (μm)	Intensity (km mol^{-1})
70.484	2.714	15.755	2.604	10.034	53.319	6.332	23.579
57.020	7.408	15.572	23.439	9.895	96.836	6.228	6.793
50.455	4.871	15.359	12.316	9.820	234.609	6.005	41.042
46.298	4.343	15.213	61.124	9.747	110.974	5.387	18.220
45.221	4.878	15.109	19.163	9.661	115.676	5.231	2.832
45.013	12.676	14.821	5.943	9.628	45.308	5.227	39.017
42.249	3.256	14.714	20.707	9.566	26.118	5.188	4.913
40.093	4.512	14.659	9.323	9.554	113.140	5.178	60.208
37.083	5.313	14.518	22.481	9.482	23.876	5.147	7.977
36.768	4.862	14.326	3.868	9.382	116.885	5.112	6.839
34.721	20.905	14.220	5.266	9.326	19.232	5.096	94.773
33.297	14.692	14.054	20.588	9.291	68.690	5.090	101.302
32.892	4.518	13.983	11.080	9.203	83.438	5.079	10.908
30.462	8.696	13.836	4.819	9.109	22.454	5.065	4.064
29.129	3.976	13.792	16.252	9.022	105.420	5.003	100.868
28.368	11.293	13.569	10.434	9.009	110.487	4.975	54.379
27.788	23.881	13.523	53.069	8.869	105.885	4.971	113.044
25.232	10.288	13.441	48.453	8.664	24.228	4.953	140.436
24.425	84.131	13.339	4.836	8.543	116.443	4.934	45.315
24.179	50.943	13.271	16.988	8.503	76.369	4.906	48.823
23.539	28.586	13.182	38.362	8.455	10.287	4.900	13.022
23.103	14.36 1	12.928	22.052	8.363	26.585	4.879	11.338
22.050	10.682	12.886	21.105	8.334	11.198	4.828	100.180
21.906	31.207	12.747	59.203	8.213	16.082	4.593	11.067
21.473	25.968	12.723	29.621	8.095	32.949	4.377	345.287
20.984	79.193	12.655	89.682	7.919	32.797	4.372	167.467
20.616	25.595	12.580	49.768	7.907	77.750	4.295	53.979
20.455	16.582	12.487	28.215	7.785	42.381	4.288	10.133
19.903	3.373	12.419	100.261	7.681	13.564	4.273	44.411
19.520	5.584	12.317	137.383	7.557	36.381	4.194	222.370
19.255	7.765	12.240	192.146	7.296	50.272	4.180	392.563
19.088	14.444	12.161	67.349	7.224	60.498	4.176	88.638
18.678	13.223	12.095	62.937	7.189	3.032	4.147	278.499
18.564	16.996	11.784	93.512	7.143	6.248	4.133	76.476
18.271	10.651	11.661	92.412	7.085	15.887	4.050	352.226
18.133	12.718	11.433	58.935	7.024	54.520	3.946	65.796
17.936	6.649	11.113	27.914	6.973	18.399	3.866	98.050
17.890	22.082	10.854	150.226	6.885	14.362	3.854	169.623
17.238	7.295	10.737	124.702	6.844	5.448	3.849	238.873
17.088	11.490	10.511	204.345	6.768	16.451	3.793	69.196
16.858	6.842	10.292	337.588	6.673	40.457	3.751	91.593
16.765	40.762	10.181	327.461	6.574	29.044	3.601	237.929
16.333	20.843	10.159	59.929	6.529	13.808		
16.099	28.915	10.108	146.893	6.422	43.568		

Table S3. Infrared bands and intensities for Fe_3H_{25}. Only bands with intensities above 2 km mol^{-1} are shown.

Band (μm)	Intensity (km mol^{-1})	Band (μm)	Intensity (km mol^{-1})
83.662	2.516	10.836	53.799
56.303	9.143	9.986	15.568
49.230	18.609	9.684	197.290
43.906	18.599	9.614	26.290
39.161	11.289	9.495	122.583
35.955	4.639	9.153	48.275
35.075	6.355	9.116	153.497
32.489	24.243	8.896	24.220
31.354	16.930	8.827	40.978
30.722	3.996	8.729	160.651
29.519	33.188	8.699	59.320
28.926	2.998	8.243	50.655
27.174	3.229	7.636	130.980
25.855	17.867	7.179	15.297
24.742	9.958	7.032	118.927
24.311	4.998	6.935	231.976
23.741	5.680	6.688	237.549
22.184	10.948	6.188	5.885
21.612	14.462	5.854	4.895
18.847	20.441	5.809	23.723
18.111	71.394	5.639	10.266
17.016	55.199	5.536	61.879
16.912	25.146	5.496	11.737
16.472	31.744	5.424	7.760
16.088	19.281	5.378	3.222
15.619	32.282	5.360	3.794
15.427	56.003	5.214	2.513
15.080	46.897	5.100	67.315
14.836	11.827	5.053	40.754
14.388	55.554	4.061	144.049
14.370	96.957	4.048	186.391
14.133	56.047	4.023	100.385
13.523	4.067	3.765	194.473
13.415	82.563	3.653	124.806
12.871	10.453	3.645	144.024
12.588	92.607	3.635	86.744
12.106	13.944	3.498	120.231
11.935	17.547	3.479	145.826
10.991	23.095		

Table S4. Infrared bands and intensities for Fe_4H_{25}. Only bands with intensities above 2 km mol^{-1} are shown.

Band (μm)	Intensity (km mol^{-1})	Band (μm)	Intensity (km mol^{-1})
107.133	44.221	9.791	134.812
68.859	8.595	9.682	10.633
44.475	15.409	9.255	180.494
43.580	8.040	9.192	73.073
41.612	16.569	9.078	18.873
36.492	6.366	8.962	24.004
34.547	8.378	8.879	32.242
33.409	9.230	8.773	46.272
30.858	24.975	8.711	46.673
29.952	8.000	8.489	17.769
29.406	4.173	8.339	4.395
27.359	2.838	8.047	22.475
25.824	23.120	7.172	7.806
24.781	45.523	7.136	15.999
22.243	26.893	7.062	48.070
21.832	8.105	6.671	21.170
21.234	8.517	6.526	3.218
20.447	24.236	6.362	4.361
19.856	32.659	5.740	2.892
19.539	5.709	5.721	21.132
18.800	33.036	5.564	7.898
18.182	23.299	5.383	10.790
17.099	6.212	5.360	7.641
16.064	96.373	5.356	26.395
15.684	24.778	5.229	11.211
15.485	35.924	5.191	36.792
14.854	2.467	5.132	144.669
14.744	41.193	5.116	7.849
14.180	87.340	5.080	30.734
13.748	16.051	4.990	140.327
13.676	18.555	4.045	88.070
13.444	2.808	3.933	159.488
13.185	42.963	3.894	125.524
12.679	100.206	3.870	171.262
12.464	10.310	3.753	127.317
10.813	30.523	3.721	158.850
10.407	254.551	3.673	352.667
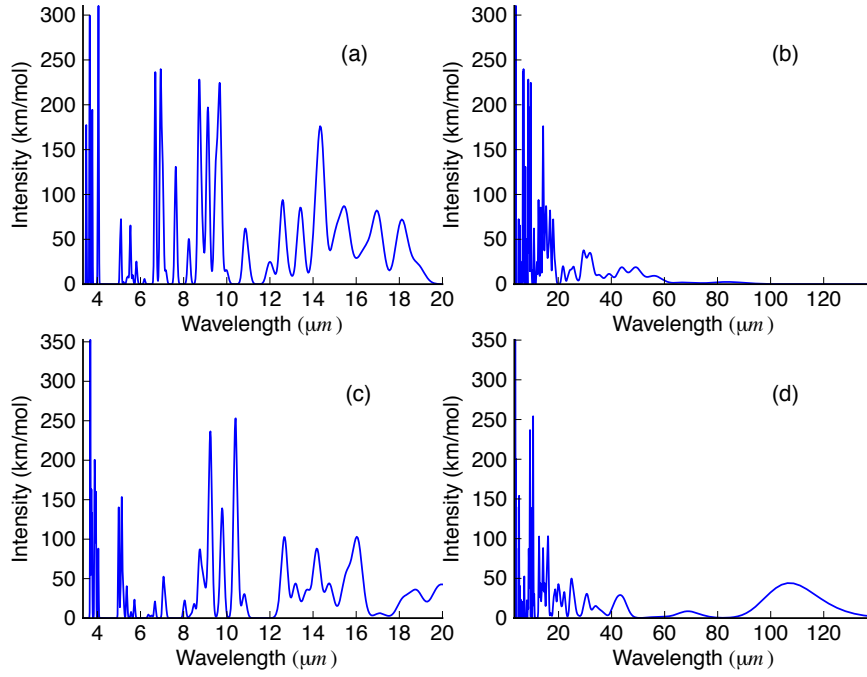
Figure S1. IR spectra of: (a) Fe_3H_{25}, (b) Fe_3H_{25} including far-IR, (c) Fe_4H_{25}, (d) Fe_4H_{25} including far-IR.